INTERNATIONAL JOURNAL FOR NUMERICAL METHODS IN FLUIDS, VOL. 20, 1273–1288 (1995)

FRACTIONAL STEP METHOD FOR SOLUTION OF INCOMPRESSIBLE NAVIER–STOKES EQUATIONS ON UNSTRUCTURED TRIANGULAR MESHES

G. K. DESPOTIS AND S. TSANGARIS

Laboratory of Aerodynamics, National Technical University of Athens, PO Box 64070, 15710 Zografou, Athens, Greece

SUMMARY

In this paper an implicit fractional step method for the solution of the two-dimensional, time-dependent, incompressible Navier–Stokes equations is presented. The current method was developed for use on an unstructured grid made up of triangles. The basic principles of this method are that the evaluation of the time evolution is split into intermediate steps and that for the spatial discretization of the flow equations a finite volume discretization on an unstructured triangular mesh is used. The present approach has been used to simulate viscous, laminar flows for various Reynolds numbers in test cases such as a backward-facing step, a square cavity and a channel with wavy boundaries.

KEY WORDS: Navier–Stokes equations; unstructured; finite volume; incompressible

1. INTRODUCTION

During the last decade there have been many papers published internationally on methods, techniques and algorithms that numerically solve the momentum and continuity equations for flow problems using unstructured meshes.

Numerical algorithms for the solution of the governing compressible fluid flow equations on unstructured meshes have been developed in recent years.[1–5] These unstructured algorithms are based on the finite volume method and simulate the viscous and inviscid flows around simple geometries (such as single aerofoils) and also around complicated geometries (such as a two-element high-lift aerofoil/flap configuration).

Solution algorithms for the incompressible Navier–Stokes equations on unstructured meshes have also evolved rapidly in recent years. Most of these algorithms[6–8] are based on the finite element method but a few[9–11] are based on the covolume method. The complementary volumes or covolumes consist of dual sets of control volumes. The covolumes have the following property: the edges of both sets of control volumes are perpendicular to the faces of the other set of control volumes. The simplest example consists of two sets of squares of the same size, where the corners of one of the sets are positioned at the centres of the other and the relation is mutual. These solutions algorithms[9,10] simulate the flow in simple and complicated channel geometries, such as the flow in a square cavity, the flow in an obstructed channel that is used in gas turbines as labyrinth seals, the flow in packed-bed reactors that are used in automobiles for the catalytic oxidation of engine exhaust emissions, etc. The article by Choudhury and Nicolaides[11] focuses on the vorticity–velocity formulation for planar incompressible flows.

CCC 0271–2091/95/111273–16

Received 28 August 1992
Revised 31 August 1993

In this work the Chorin fractional step method[12] is used to simulate two-dimensional, incompressible, viscous, laminar flows. The Chorin method is adapted to the basic flow equations by splitting the former into two intermediate steps. The new element in this work is that while in the original Chorin method an explicit first-order scheme in time is used and the spatial discretization depends on the finite difference mesh, known as the MAC mesh, here an implicit first-order scheme in time is used and for the spatial discretization of the governing equations a finite volume approximation on an unstructured triangular mesh is applied. The control volumes used are the triangle and the polygon, which are single control volumes, in contrast with the complementary control volumes.

The paper is organized as follows: Section 2 discusses the method used for the solution of the flow equations, the boundary conditions and the computing procedure. In Section 3 the discretization of the flux terms, diffusive terms and Poisson equation is discussed. Finally, the method is applied for the prediction of the flow over a wide range of wall geometries. The flow over a backward-facing step is examined for two different Reynolds numbers (Re = 67 and 200) and the results are compared with the numerical results of other researchers. The flow in a square cavity is also examined for three different Reynolds numbers (Re = 100, 400 and 3200) for which numerical results and experimental data are available. Finally, the flow in a channel with wavy boundaries is studied for a Reynolds number equal to 10 and the results are compared with the analytical solutions.

2. GOVERNING EQUATIONS

The momentum and continuity equations of an incompressible viscous fluid are written in dimensionless form as

$$\frac{\partial u_i}{\partial t} + \frac{\partial}{\partial x_j}(u_i u_j) = -\frac{\partial p}{\partial x_i} + \frac{1}{Re}\frac{\partial^2 u_i}{\partial x_j \partial x_j}, \tag{1}$$

$$\frac{\partial u_i}{\partial x_i} = 0, \tag{2}$$

where u_i denotes the velocity component in the x_i-direction in a Cartesian co-ordinate system, p is the pressure and Re is the Reynolds number of the flow. It should be noted that the convective terms in the momentum equation (1) are written in conservative form.

The proposed method has been developed by Chorin.[12] In the explicit version of the fractional step method described by Chorin an explicit first-order scheme in time is used. The spatial discretization depends on the actual finite difference mesh consisting of quadrilateral elements. While Chorin used a non-staggered grid in his implicit version of the fractional step method, Andersson and Kristoffersen[13] defined the dependent variables on the staggered grid positions with a similar implicit fractional step method. On the staggered grid the values of the velocities are evaluated at the middle of a cell's faces and the value of the pressure at the centre of the cell. This mesh distribution is known as the MAC mesh.[14]

In the current fractional step method an implicit first-order scheme in time is used with respect to the convective and diffusive terms. Now the method is adapted to the basic equations (1) and (2) by splitting the former into two intermediate steps:

$$\frac{u_i^* - u_i^n}{\Delta t} + \frac{\partial}{\partial x_j}\left(u_j^n u_i^*\right) = \frac{1}{Re}\frac{\partial^2 u_i^*}{\partial x_j \partial x_j}, \tag{3}$$

$$\frac{u_i^{n+1} - u_i^*}{\Delta t} + \frac{\partial p^{n+1}}{\partial x_i} = 0, \tag{4}$$

where u_i^* is an intermediate or tentative value of the velocity component and the superscript n denotes the solution at time $t = n\Delta t$, the time step being Δt. Thus, if the solution tends to a steady state, the velocity u_i^{n+1} at the new time level becomes equal to u_i^n according to equations (3) and (4).

An essential feature of the decomposition (3), (4) is that the tentative velocity u_i^* can be calculated implicitly from equation (3), while the new velocity u_i^{n+1} is related to the new pressure field p^{n+1} equation (4). By taking the divergence of equation (4) and making subsequent use of the incompressibility condition (2) for u_i^{n+1}, we obtain the Poisson equation

$$\frac{\partial^2 p^{n+1}}{\partial x_j \partial x_j} = \frac{1}{\Delta t} \frac{\partial u_i^*}{\partial x_i}. \tag{5}$$

Thus, with p^{n+1} known from the solution of equation (5), the velocities of the new time level $n+1$ are readily derived from equation (4) as

$$u_i^{n+1} = u_i^* - \Delta t \frac{\partial p^{n+1}}{\partial x_i}. \tag{6}$$

For the spatial discretization of the governing equations a finite volume approximation on an unstructured triangular mesh is used. On the triangular mesh the velocities are stored at the nodes of the triangular cell and the pressure at the centre of it. Using the finite volume technique on an unstructured triangular mesh, the flux terms are calculated at the nodes and across the edges of the triangular cell and the diffusive terms at the nodes.

A structured triangular grid, i.e. constructed using interpolations, is used for the numerical solution of the flow equations, but the current algorithm considers it as unstructured. For structured grids, mesh co-ordinate directions can be identified and used to number the cells and nodes. Thus a cell may be identified by its two indices I and J in the mesh co-ordinate system and its neighbours may be located by incrementing one of these indices. However, for unstructured meshes this is no longer possible, since in principle the cells and nodes are ordered randomly. Thus the use of unstructured meshes requires the storage of connectivity information along with the use of an indirect addressing system.

Since flux and diffusive terms are to be calculated at each point of the mesh, a data structure based on the mesh points can be employed. To define a point-based structure, 18 integer addresses must be stored for each point. Thus an array must be dimensioned $KNU(KMAX \times 18)$, where $KMAX$ is the total number of points in the mesh. For each point the first 12 values in KNU correspond to the addresses of the 12 neighbouring points of that point and the other six values correspond to the addresses of the six triangular cells which have that point as a common vertex.

For the above-mentioned test cases four types of boundaries are used: inflow boundary, outflow boundary, solid surfaces and symmetry axis. For each type and for each unknown let us see what boundary conditions are to be specified.

Boundary conditions for the velocities

Inflow boundary. Here we apply a uniform or fully developed profile for the u-velocity, while the v-velocity is set to zero:

$$u = \text{const.} \quad \text{or} \quad u = u(y), \qquad v = 0.$$

Outflow boundary. Here we apply the fully developed flow conditions

$$\frac{\partial u}{\partial x} = \frac{\partial v}{\partial x} = 0.$$

Symmetry axis. We apply symmetry conditions. Both the first-order derivative of the u-component of the velocity in the y-direction and the v-component of the velocity are set to zero:

$$\frac{\partial u}{\partial y} = 0, \qquad v = 0.$$

Solid surfaces. We apply non-slip conditions:

$$u = v = 0.$$

Boundary conditions for the pressure

The boundary conditions imposed on p are consistent with equation (4). Thus, if we take

$$u_i^* = u_i^{n+1} \tag{7}$$

on a boundary with its normal along the x_i-direction, equation (6) becomes

$$\frac{\partial p^{n+1}}{\partial x_i} = 0, \tag{8}$$

i.e. zero normal derivative of p^{n+1} on the boundary.

The boundary value problem given by the Poisson equation (5) subject to the Neumann boundary condition (8) is an interior Neumann problem for the three-dimensional case, for which

$$\int\int\int_V \frac{\partial u_i^*}{\partial x_i}\, \mathrm{d}V = 0 \tag{9}$$

is a necessary condition for a solution to exist. By using Gauss's theorem, the compatibility condition (9) becomes

$$\int\int_S u_i^* n_i \, \mathrm{d}S = 0, \tag{10}$$

where n_i denotes the components of the unit normal vector to the boundary S of the calculation domain V. Thus, by introducing equation (7) in the surface integral (10), it is observed that compatibility is automatically achieved provided that the boundary conditions on u_i^{n+1} assure zero net flux into the calculation domain.

Around the computational domain there are 'pseudocells' that are used for the implementation of the boundary conditions. This is necessary because the pressure is calculated at the centre of the triangular cell and the flux terms are calculated across the edges of it.

In summary, the present solution algorithm consists of the following basic steps.

1. An initial field for velocity and pressure is applied.
2. The momentum equations are solved and a velocity field that does not fulfil the continuity equation is achieved. The solution of the momentum equation is obtained using the Gauss–Seidel method.
3. The Poisson equation is solved and a pressure field is calculated. The solution of the Poisson equation is also obtained using the Gauss–Seidel method.
4. The velocity components at the new time step level are evaluated from equation (4). If convergence of the velocity and pressure is achieved, the calculation of the flow field is completed. Convergence is achieved if the residuals are less than 10^{-4}.

3. NUMERICAL SOLUTION

In this work the Navier–Stokes equations are integrated in time using an implicit first-order time-stepping scheme. These equations are integrated in space using a finite volume method developed for an unstructured grid made up of triangles. For the integration around a finite volume the derivatives of the flow equations must be converted into closed line integrals using some formulation of the Stokes theorem, which is described by the following equation:

$$\int_S \vec{\alpha} \cdot \mathrm{d}\vec{r} = \int_E \mathrm{rot}\vec{\alpha} \cdot \vec{n}\, \mathrm{d}E,$$

where $\mathrm{d}\vec{r}$ is the elementary arc, $\mathrm{d}E$ is the elementary surface and $\vec{n}$ is the normal vector to this surface.

Two finite volumes are used, triangle and polygon, because the pressure is calculated at the centre of the triangular cell and the velocities at the nodes of it. Thus two such finite volume discretization schemes have been adapted, the cell-centred scheme and the nodal scheme.

3.1. Discretization of flux terms at polygon centre

In this case the velocities are stored at the nodes of the polygon and the flux terms are calculated at the node c (see Figure 1). The nodal finite volume discretization scheme[15] is used for the discretization of the flux terms that appear in the momentum equations (convective terms). The first differences are computed as

$$\left(\frac{\partial U}{\partial x}\right)_c = \frac{1}{A_c}\int_{S_c} U\,\mathrm{d}y = \frac{1}{A_c}\sum_{i=1}^{6}\frac{U_{i+1}+U_i}{2}(y_{i+1}-y_i),$$

$$\left(\frac{\partial U}{\partial y}\right)_c = -\frac{1}{A_c}\int_{S_c} U\,\mathrm{d}x = -\frac{1}{A_c}\sum_{i=1}^{6}\frac{U_{i+1}+U_i}{2}(x_{i+1}-x_i),$$

where A_c is the area of the polygonal control volume (1–2–3–4–5–6) (see Figure 1), U is the component of the fluxes, x and y are the co-ordinates of the polygon vertices and i refers to the six vertices of the polygonal control volume.

In Figures 1–5 the numbers without parentheses refer to the index of the equations and the numbers in parentheses denote the same locations of Figure 3. In the same figures (P) and (U) denote the locations of pressure and velocity nodes respectively.

The closed line integral is approximated by the trapezoidal integration rule: for each edge delimiting

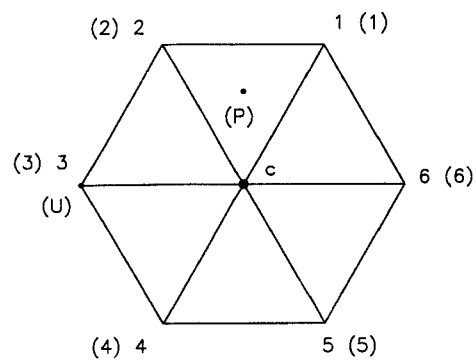

Figure 1. Equivalent control volume for finite volume approximation to flux terms at polygon centre

the control volume boundary, the contribution to the closed line integral is obtained by evaluating the velocities at the nodes on both ends of the edge and taking the scalar product of their averaged value with the directed length of the edge. This discretization can be shown to be equivalent to a finite element Galerkin approximation,[15] which is known to be second-order-accurate in space for a mesh consisting of equilateral triangles.

3.2. *Discretization of flux terms at triangle centre*

In this case the spatial discretization procedure begins by storing the velocities at the vertices of the triangular cells. The flux terms must be calculated at the centres of the triangles (see Figure 2). This is achieved by computing the required first differences for the velocities at the triangle centres.[4] For a piecewise linear approximation of the velocities in space the first differences are constant over each triangle and are computed as

$$\left(\frac{\partial U}{\partial x}\right)_K = \frac{1}{A_K}\int_{S_K} U\,\mathrm{d}y = \frac{1}{A_K}\sum_{i=1}^{3}\frac{U_{i+1}+U_i}{2}(y_{i+1}-y_i),$$

$$\left(\frac{\partial U}{\partial y}\right)_K = -\frac{1}{A_K}\int_{S_K} U\,\mathrm{d}x = -\frac{1}{A_K}\sum_{i=1}^{3}\frac{U_{i+1}+U_i}{2}(x_{i+1}-x_i),$$

where A_K is the area of the triangular control volume (1–2–3) (see Figure 2), U is the component of the velocity and the summation over i refers to the three vertices of the triangle.

Generally the nodal finite volume scheme is used for the discretization of the derivatives of the velocity that appear on the right-hand side of the Poisson equation, but in this case the control volume is not polygonal but triangular. The closed line integral is approximated in the same manner as described in Section 3.1.

3.3. *Discretization of diffusive terms at polygon centre*

The spatial discretization procedure begins by storing the velocities at the vertices of the polygon (1–2–3–4–5–6) and at the vertices of the neighbouring triangles (see Figure 3). The diffusive terms must be calculated at the node c and this is achieved by computing the second-order derivatives at the same point. The required second differences may be computed as

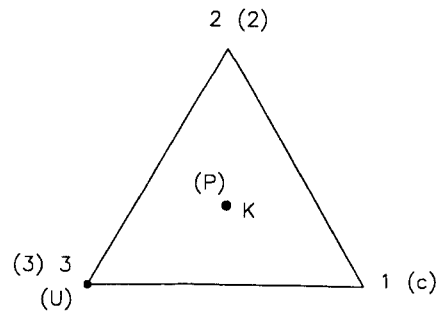

Figure 2. Equivalent control volume for finite volume approximation to flux terms at triangle centre

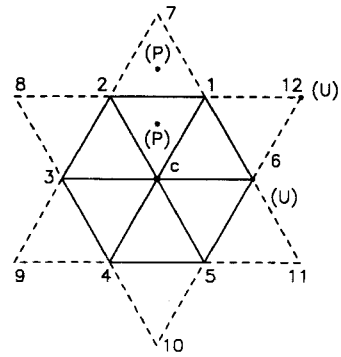

Figure 3. Equivalent control volume for finite volume approximation to diffusive terms at polygon centre

$$\left(\frac{\partial^2 U}{\partial x^2}\right)_c = \left[\frac{\partial}{\partial x}\left(\frac{\partial U}{\partial x}\right)\right]_c = \frac{1}{A_c}\int_{S_c}\frac{\partial U}{\partial x}\,dy = \frac{1}{A_c}\sum_{i=1}^{6}\left(\frac{\partial U}{\partial x}\right)_{i+1/2}(y_{i+1}-y_i),$$

$$\left(\frac{\partial^2 U}{\partial y^2}\right)_c = \left[\frac{\partial}{\partial y}\left(\frac{\partial U}{\partial y}\right)\right]_c = -\frac{1}{A_c}\int_{S_c}\frac{\partial U}{\partial y}\,dx = -\frac{1}{A_c}\sum_{i=1}^{6}\left(\frac{\partial U}{\partial y}\right)_{i+1/2}(x_{i+1}-x_i),$$

where A_c denotes the area of the polygonal control volume, U denotes the component of the velocity, i refers to the six vertices of the polygon and $i+\frac{1}{2}$ refers to the six middles of the edges of the polygon.

The viscous components involve the evaluation of derivatives of the primitive variables (velocities) on each polygonal contour. To be consistent with the overall contour integral method of evaluating derivatives, it remains to define a suitable contour for obtaining first derivatives on edges. There is no unique way to perform the integration, but perhaps the simplest is to use the contour shown in Figure 4, so that the derivative at the middle of the edge is the sum of four terms.[5] The first differences at the middle of the edge are defined as

$$\left(\frac{\partial U}{\partial x}\right)_{i+1/2} = \frac{1}{A}\int_S U\,dy = \frac{1}{A}\sum_{j=1}^{4}\frac{U_{j+1}+U_j}{2}(y_{j+1}-y_j),$$

$$\left(\frac{\partial U}{\partial y}\right)_{i+1/2} = -\frac{1}{A}\int_S U\,dx = -\frac{1}{A}\sum_{j=1}^{4}\frac{U_{j+1}+U_j}{2}(x_{j+1}-x_j),$$

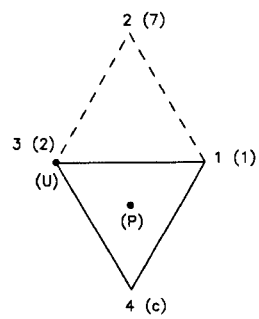

Figure 4. Equivalent control volume for finite volume approximation to first-order derivative of velocity at middle of polygon edge

where A is the sum of the areas of the two adjacent triangles which define the contour, U is the velocity component and the summation over j refers to the four vertices of the quadrilateral.

The nodal finite volume scheme, which is used for discretization of the first and second differences and the overall contour integral, is approximated in the same way as described in Section 3.1.

3.4. *Discretization of first-order pressure terms at triangle centre*

The cell-centred finite volume scheme[2] is used for discretization of the first-order pressure terms, which are calculated at the centre of the triangular control volume (1–2–3) (see Figure 5). The first differences are defined as

$$\left(\frac{\partial P}{\partial x}\right)_K = \frac{1}{A_K}\int_{S_K} P\,\mathrm{d}y = \frac{1}{A_K}\sum_{i=j=1}^{3}\frac{P_K + P_j}{2}(y_{i+1} - y_i),$$

$$\left(\frac{\partial P}{\partial y}\right)_K = -\frac{1}{A_K}\int_{S_K} P\,\mathrm{d}x = -\frac{1}{A_K}\sum_{i=j=1}^{3}\frac{P_K + P_j}{2}(x_{i+1} - x_i),$$

where A_K denotes the area of the triangular control volume, P denotes the pressure, i refers to the three vertices of the triangular cell and j refers to the centres of the three neighbouring triangles.

The pressure is stored at the centre of each cell and assumed to represent an average value over the entire control volume. In order to evaluate the closed line integral, estimates of the pressure along the edges of the triangular cell are needed. These are taken as the average of the values at both cells on either side of that edge. This is the equivalent of central differencing on a Cartesian grid and is second-order-accurate for a mesh that consists of equilateral triangles.

3.5. *Discretization of second-order pressure terms at triangle centre*

The second-order pressure terms that are present on the left-hand side of the Poisson equation are also calculated at the centre K of the triangular control volume (1–2–3) (see Figure 5). These calculations require the evaluation of second differences of pressure at the same point K. The second-order derivatives of pressure may be computed as

$$\left(\frac{\partial^2 P}{\partial x^2}\right)_K = \left[\frac{\partial}{\partial x}\left(\frac{\partial P}{\partial x}\right)\right]_K = \frac{1}{A_K}\int_{S_K}\frac{\partial P}{\partial x}\,\mathrm{d}y = \frac{1}{A_K}\sum_{i=j=1}^{3}\frac{(P_x)_K + (P_x)_j}{2}(y_{i+1} - y_i),$$

$$\left(\frac{\partial^2 P}{\partial y^2}\right)_K = \left[\frac{\partial}{\partial y}\left(\frac{\partial P}{\partial y}\right)\right]_K = -\frac{1}{A_K}\int_{S_K}\frac{\partial P}{\partial y}\,\mathrm{d}x = -\frac{1}{A_K}\sum_{i=j=1}^{3}\frac{(P_y)_K + (P_y)_j}{2}(x_{i+1} - x_i),$$

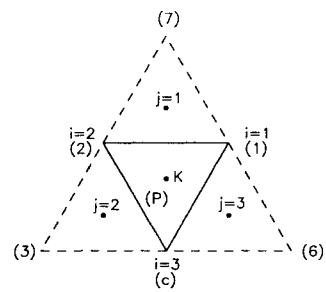

Figure 5. Equivalent control volume for finite volume approximation to first- and second-order pressure terms at triangle centre

where A_K, P, i and j are the same as defined Section 3.4 and P_x and P_y are the x and y first-order derivatives of pressure respectively.

For the evaluation of second differences of pressure the cell-centred finite volume discretization scheme is also used, but the first-order derivatives of pressure must be known. These can be evaluated according to Section 3.4.

4. RESULTS AND VALIDATION

4.1. *Flow over a backward-facing step*

In this case the flow over a backward-facing step for two different Reynolds numbers, $Re = 67$ and 200, is examined. The Reynolds number is calculated from

$$Re = \frac{U_{\text{ref}} L_{\text{ref}}}{\nu_{\text{ref}}}, \tag{11}$$

where U_{ref} is the mean velocity at the channel inlet, L_{ref} is the height H of the second part of the channel (see Figure 6) and ν_{ref} is the reference kinematic viscosity.

Figure 6 shows the geometric characteristics of the backward-facing step and the grid used. This grid is the same for both Reynolds numbers and consists of 3402 nodes. The dimensionless length of the first part of the channel is $1 = 3$, its dimensionless height is $h = 0{\cdot}5$, the total dimensionless length of the channel is $L = 15$ and the dimensionless height of the second part is $H = 1$. The dimensionless profile of axial velocity at the inflow boundary is given by

$$u = \frac{3}{2}\left[1 - \left(\frac{y - h/2}{h/2}\right)^2\right].$$

In Figure 7 the steady u-component of the velocity as a function of the normalized co-ordinate $y/(H - h)$ is shown at several x-locations, $x = 2{\cdot}3$, $3{\cdot}4$, 4 and 5, for $Re = 67$. In Figure 8 the u-component of the velocity at the same positions of the channel is shown for $Re = 200$. The time step $\Delta t = 0{\cdot}009$ is used for both Reynolds numbers. The profiles plotted with a solid line are the results of the current method and the rest of the profiles are numerical results of other researchers.[16,17]

4.2. *Flow in a square cavity*

In this case the flow in a square cavity for three different Reynolds numbers, $Re = 100$, 400 and 3200, is examined. The Reynolds number is calculated using equation (11), where U_{ref} is the fluid velocity of the moving boundary and L_{ref} is the length of the side of the square cavity. Figure 9 shows the grid used for $Re = 100$ and 400, which consists of 1654 nodes. For $Re = 3200$ a similar grid consisting of 14,996 nodes is used. The dimensionless u-velocity profile at the top boundary is $u = 1$ and for the other boundaries the no-slip conditions are applied.

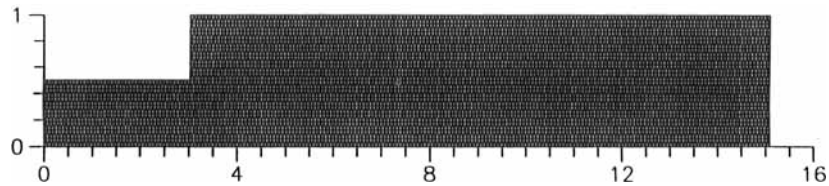

Figure 6. Grid for backward-facing step

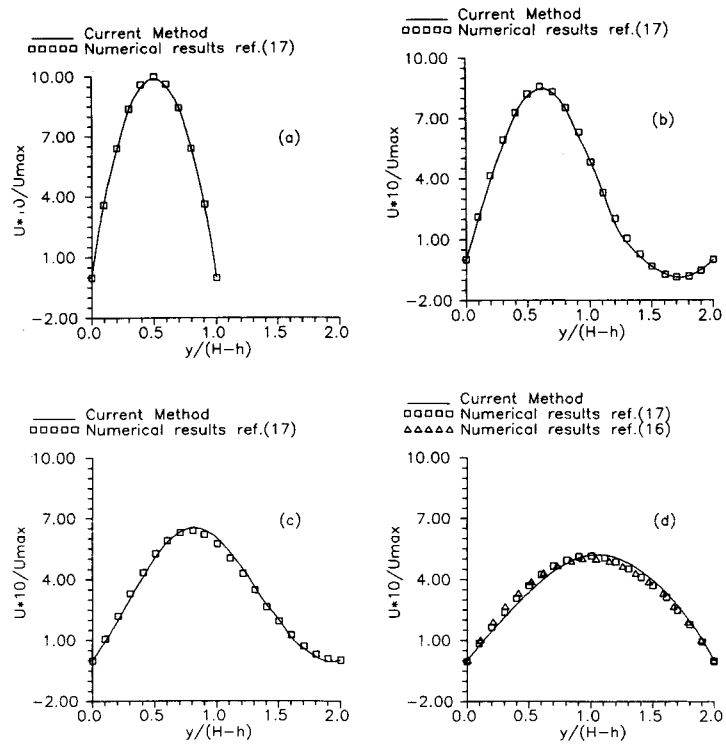

Figure 7. Comparison of u-velocity profiles for $Re = 67$: (a) $x = 2{\cdot}3$, (b) $x = 3{\cdot}4$, (c) $x = 4{\cdot}0$, (d) $x = 5{\cdot}0$

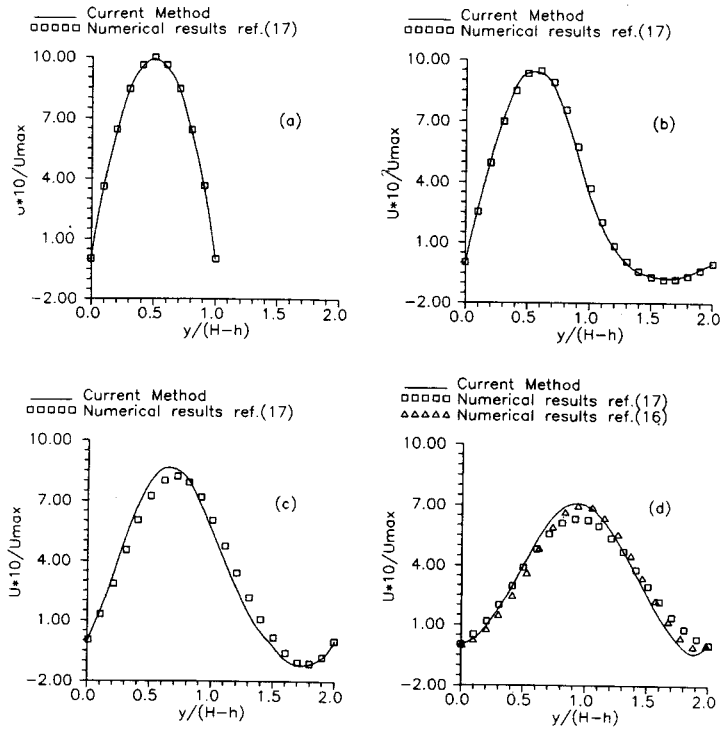

Figure 8. Comparison of u-velocity profiles for $Re = 200$: (a) $x = 2{\cdot}3$, (b) $x = 3{\cdot}4$, (c) $x = 4{\cdot}0$, (d) $x = 5{\cdot}0$

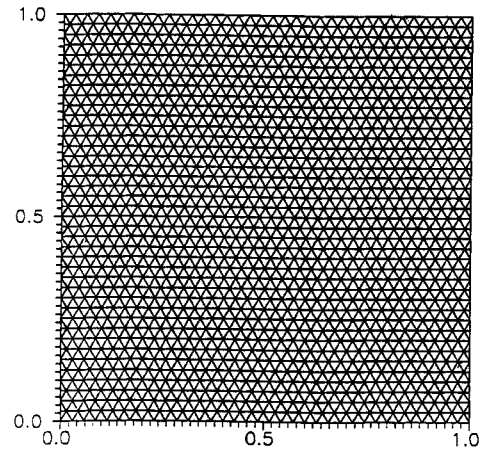

Figure 9. Grid for square cavity ($Re = 100$ and 400)

Figure 10 shows the velocity profiles for u along a vertical line passing through the geometric centre of the cavity for $Re = 100$, 400 and 3200. The time steps used are $\Delta t = 0{\cdot}007$ for $Re = 100$ and 400 and $\Delta t = 0{\cdot}001$ for $Re = 3200$. The results of the current method are plotted with a solid line, the numerical results of other researchers[18,19] with a broken line and the symbols are experimental data.[20] The thinning of the wall boundary layers with increasing Reynolds number is evident from these profiles, although the rate of this thinning is slow.

The development of the flow as a function of Reynolds number is shown in Figure 11 for three conditions: $Re = 100$, 400 and 3200. As is well known, the centre of the primary vortex is offset towards the top right corner at $Re = 100$. It moves towards the geometric centre of the cavity with increasing Reynolds number.

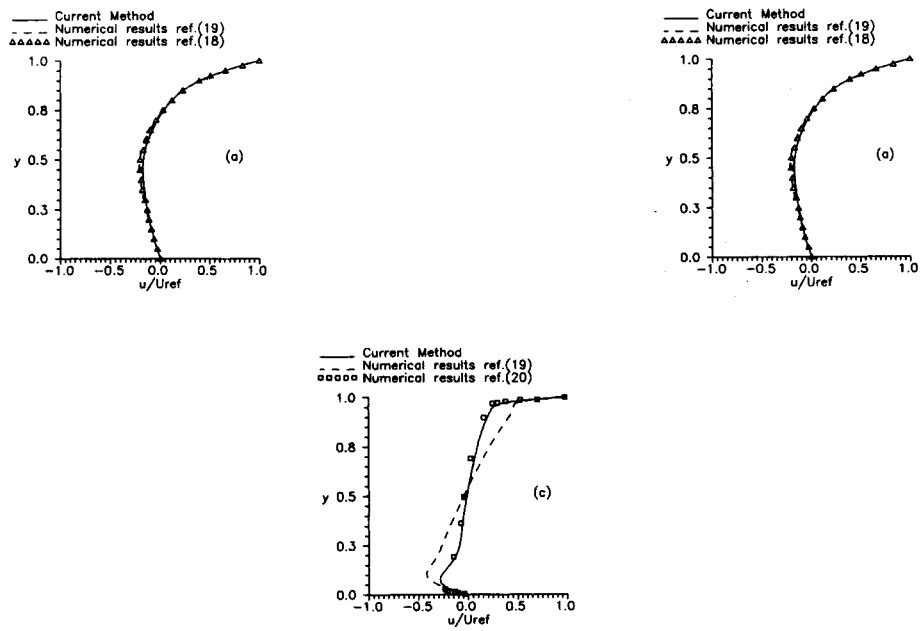

Figure 10. Comparison of u-velocity along vertical line through geometric centre: (a) $Re = 100$, (b) $Re = 400$, (c) $Re = 3200$

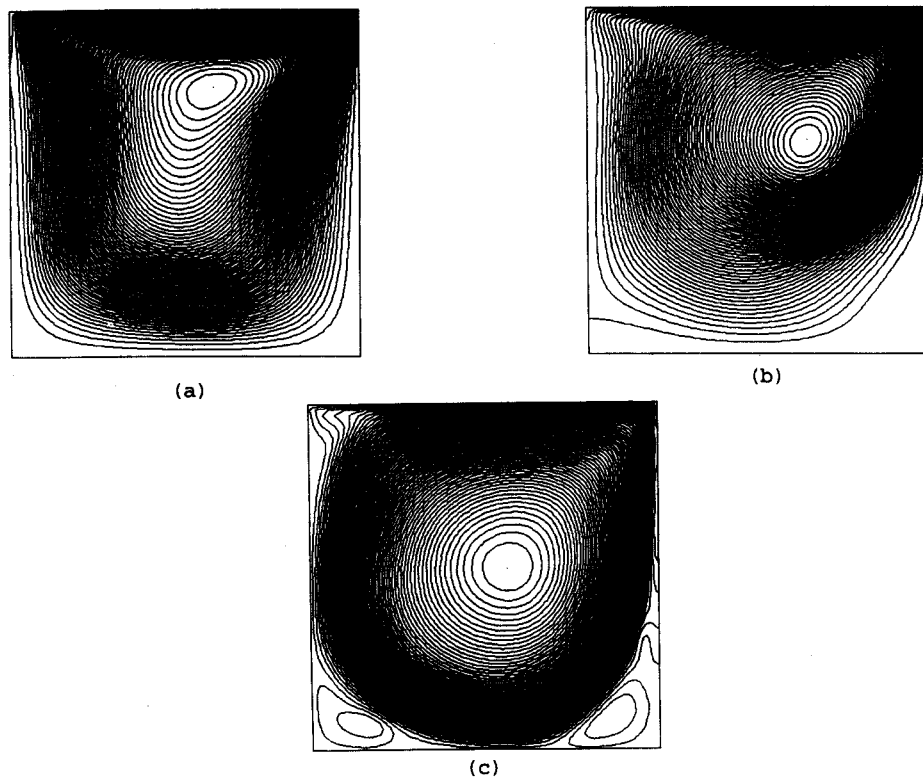

Figure 11. Streamline contours for cavity flow: (a) $Re = 100$, (b) $Re = 400$, (c) $Re = 3200$

The static and total pressure contours are shown in Figure 12. In the viscous limit (small Reynolds number) the static and total pressures show no resemblance to the streamlines. The contours cannot be closed but must end on boundaries. Conversely, for the inviscid limit (high Reynolds number) the total pressure is conserved on streamlines, so that the contours of total pressure should become identical with the streamlines. This development from viscous to inviscid flow is indicated clearly by Figure 12. From the plots we conclude that the total pressure distribution is the best indicator of the degree of viscous and inviscid flow.

Finally, Figure 13 shows the convergence history of the primitive flow variables for $Re = 100$.

4.3. Laminar steady flow in a sinusoidal channel

In this case the viscous flow past wavy boundaries is examined, which has attracted considerable interest in recent years because of the important role it plays in several phenomena: the generation of wind waves on water, the formation of sedimentary ripples in river channels and dunes in deserts, the stability of a liquid film in contact with a gas stream, and finally in biofluid mechanics. The calculation domain consists of four periods of the channel wavy boundary, described by the equation

$$y = 1 - \varepsilon(1 + \cos x).$$

In this case the coefficient is $\varepsilon = 0{\cdot}2$. In Figure 14 the grid for one period of a channel with wavy boundaries is presented, which consists of 676 nodes. The solution is performed in a channel of four periods length consisting of 2704 nodes. The flow equations for $Re = 10$ are solved. The Reynolds

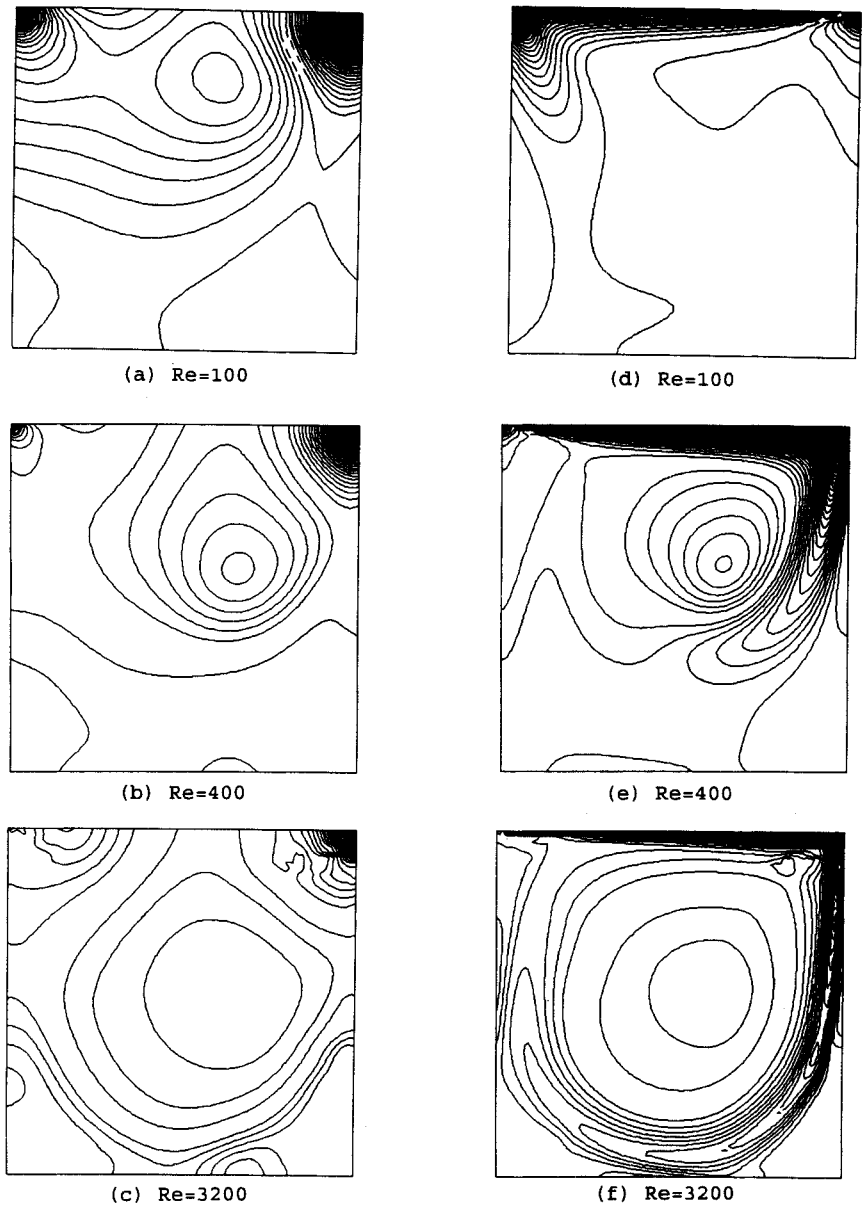

Figure 12. (a–c) Static and (d–f) total pressure contours for cavity flow

number calculation is based on equation (11). The dimensionless velocity profile at the inlet is described by

$$u = \frac{1}{h}\left[1 - \left(\frac{y}{h}\right)^2\right],$$

where $h = 0{\cdot}6$ for coefficient $\varepsilon = 0{\cdot}2$. For this case the time step used is $\Delta t = 0{\cdot}01$.

In Figure 15 the profiles of the u-component of the velocity in the same position of each period of the channel are presented. From Figure 15 it is seen that the flow periodicity is directly established. Isolating

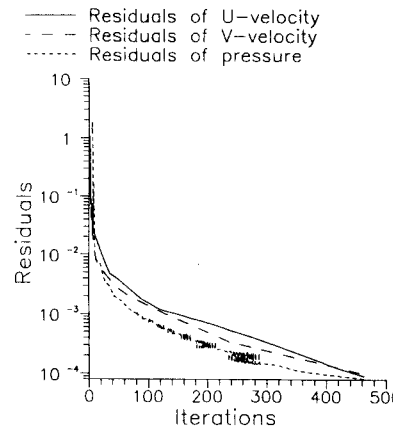

Figure 13. Convergence history for $Re = 100$

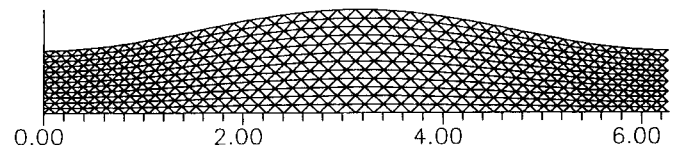

Figure 14. Grid for one period of channel with wavy boundaries

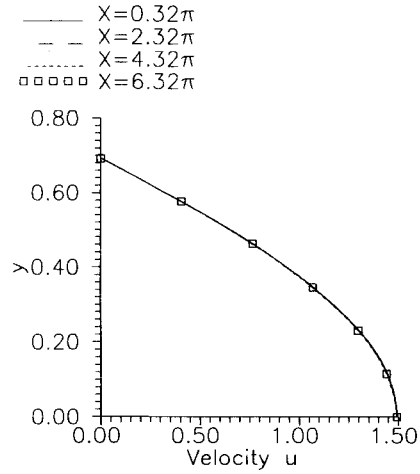

Figure 15. u-component of velocity profiles

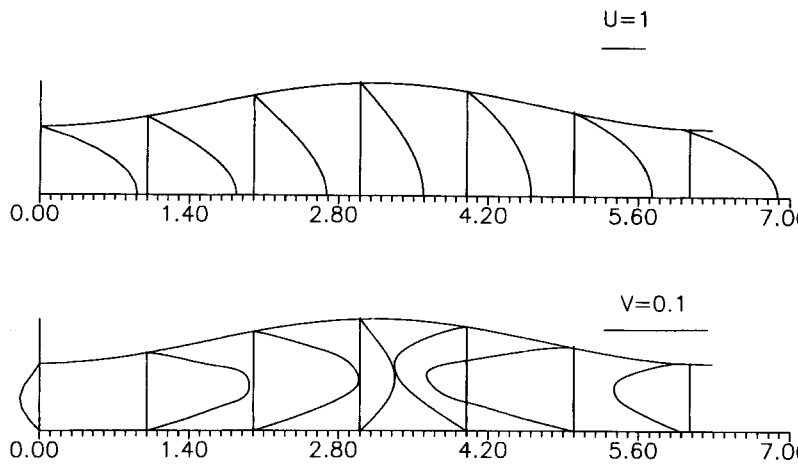

Figure 16. u-velocity (and v-velocity) profiles at various cross-sections of channel for $Re = 10$

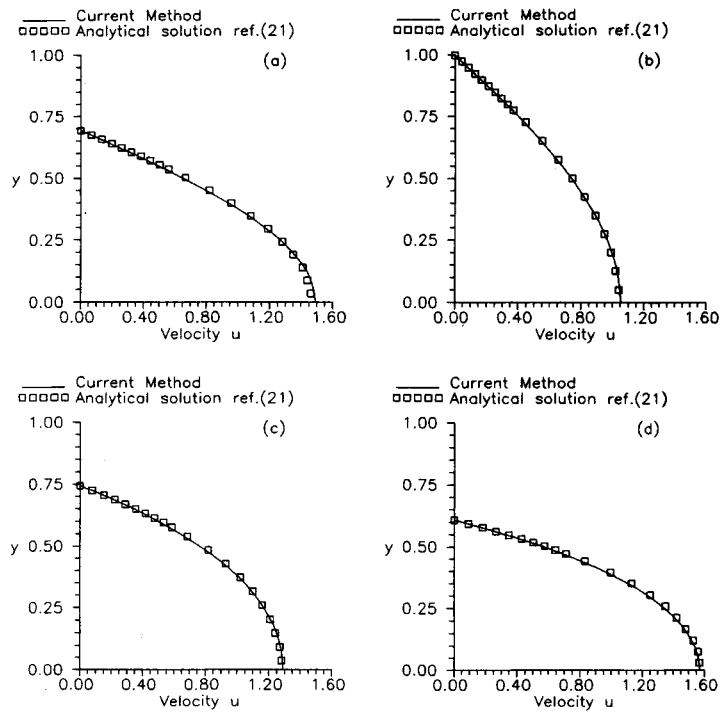

Figure 17. Comparison of u-velocity profiles for $Re = 10$: (a) $x = 1$, (b) $x = 3$, (c) $x = 5$, (d) $x = 6$

one of the channel periods, the numerical results of this method are compared with the analytical results from Reference 21. In Figure 16 the velocity profiles u and v in a channel with sinusoidal walls are shown. The velocity profiles are plotted at various cross-section of the channel, $x = 0$, 1, 2, 3, 4, 5 and 6. In Figure 17 the comparison of u-velocity profiles is shown. The profiles of the present method are plotted with a solid line, while the analytical solutions are indicated by symbols.

5. CONCLUSIONS

A novel, efficient finite volume Navier–Stokes method for unstructured grids has been developed. The current method has been validated by solving the flow over a backward-facing step, in a square cavity and in a channel with wavy boundaries and by comparing the results with the results of other researchers and other experimental data. Through the use of an unstructured grid the method is capable of computing flow fields over various geometries.

Comparing the current method with the original SOLA algorithm[22] and the Chorin method applied on an MAC mesh (original Chorin method), the conclusion drawn is that the present method requires less time to converge on a specific criterion than the SOLA algorithm but more time than the original Chorin method. Concerning the present method, about 70% of the required time is consumed by the solution of the Poisson equation, i.e. in the calculation of the pressure.

In a triangular mesh the number of triangular control volumes is almost twice the number of mesh points. This, together with the fact that the pressure is calculated at the centre of the triangular cell, explains why the current method requires more time to converge than the original Chorin method.

Solution times could always be improved if the velocities were calculated at the centre of the triangle and the pressure at its nodes.

REFERENCES

1. J. T. Batina, 'Unsteady Euler airfoil solutions using unstructured dynamic meshes', *AIAA J.*, **28**, *1381–1388 (1990).*
2. A. Jameson and D. Mavriplis, 'Finite volume solution of the two-dimensional Euler equations on regular triangular mesh', *AIAA J.*, **24**, 611–618 (1986).
3. D. J. Mavriplis, 'Multigrid solution of the two-dimensional Euler equations on unstructured triangular meshes', *AIAA J.*, **26**, 824–831 (1988).
4. D. J. Mavriplis, A. Jameson and L. Martinelli, 'Multigrid solution of the Navier–Stokes equations on triangular meshes', *AIAA Paper 89-0120*, 1989.
5. N. P. Weatherill, L. T. Johnston, A. J. Peace and J. A. Shaw, 'A method for the solution of the Reynolds-averaged Navier–Stokes equations on triangular grids', *Notes on Numer. Fluid Mech.*, **20**, 418–425 (1988).
6. D. Elkaim, M. Reggio and R. Camarero, 'Simulating two-dimensional turbulent flow by using the $k-\epsilon$ model and the vorticity–streamfunction formulation', *Int. J. Numer. methods fluids*, **14**, 961–980 (1992).
7. J. Hetu and D. H. Pelletier, 'Fast, adaptive finite element scheme for viscous incompressible flows', *AIAA J.*, **30**, 2677–2682 (1992).
8. J. Hetu and D. H. Pelletier, 'Adaptive remeshing for viscous incompressible flows', *AIAA J.*, **30**, (1992).
9. C. H. Hall, T. A. Porsching and G. L. Mesina, 'On a network method for unsteady incompressible fluid flow on triangular grids', *Int. J. numer. methods fluids*, **15**, 1383–1406 (1992).
10. C. H. Hall, T. A. Cavendish and W. H. Frey, 'The dual variable method for solving fluid flow difference equations on Delaunay triangulations', *Comput. Fluids*, **20**, 145–164 (1991).
11. S. Choudhury and R. A. Nicolaides. 'Discretization of incompressible vorticity–velocity equations on triangular meshes', *Int. J. numer. methods fluids*, **11**, 823–833 (1990).
12. A. J. Chorin, 'Numerical solution of Navier–Stokes equations', *Math. Comput.*, **22**, 745–762 (1968).
13. H. I. Andersson and R. Kristoffersen, 'Numerical simulation of unsteady viscous flows', *Arch. Mech.*, **41**, 207–223 (1989).
14. F. H. Harlow and J. E. Welch, 'Numerical calculation of time-dependent viscous incompressible flow of fluid with free surface', *Phys. Fluids*, **8**, 2182–2189 (1965).
15. A. Jameson, T. J. Baker and N. P. Weatherill, 'Calculation of inviscid transonic flow over a complete aircraft', *AIAA Paper 86-0103*, 1986.
16. H. Becker and J. Wachter, 'Numerical predictions of laminar flow behind a step', *Notes Numer. Fluid Mech.*, **9**, 48–62 (1984).
17. H. Bonnet, Y. Lecointe, J. Piquet and M. Visonneau, 'The backward-facing step comparison of two algorithms for unsteady Navier–Stokes equations', *Notes Numer. Fluid Mech.*, **9**, 63–79 (1984).
18. O. R. Burggraf, 'Analytical and numerical studies of the structure of steady separated flows', *J. Fluid Mech.*, **24**, P.1, 113–151 (1966).
19. U. Ghia, K. N. Ghia and C. T. Shin, 'High-*Re* solutions for incompressible flow using the Navier-Stokes equations and a multigrid method', *J. Comput. Phys.*, **48**, 387–411 (1982).
20. J. R. Koseff and R. L. Street, 'The lid-driven cavity flow: a synthesis of qualitative and quantitative observations', *J. Fluids Eng.*, **106**, 390–398 (1984).
21. S. Tsangaris and E. Leiter, 'On laminar steady flow in sinusoidal channels', *J. Eng. Math.*, **18**, 89–103 (1984).
22. C. W. Hirt, B. D. Nichols and N. C. Romero, 'SOLA—a numerical solution algorithm for transient fluid flows', *Los Alamos Scientific Laboratory Report LA-5852*, 1975.